Polymer 49 (2008) 2381–2386

Contents lists available at ScienceDirect

Polymer

journal homepage: www.elsevier.com/locate/polymer

Thermal properties of poly(lactic acid) fumed silica nanocomposites: Experiments and molecular dynamics simulations

Jian Zhang, Jianzhong Lou *, Shamsuddin Ilias, Parakalan Krishnamachari, Jizhong Yan

Department of Mechanical and Chemical Engineering, North Carolina A&T State University, 1601 E. Market St, Greensboro, NC 27411, USA

ARTICLE INFO

Article history:
Received 13 January 2008
Received in revised form 28 February 2008
Accepted 29 February 2008
Available online 5 March 2008

Keywords:
Molecular simulation
Nanocomposites
Biodegradable polymers

ABSTRACT

Poly(lactic acid) (PLA) fumed silica nanocomposites were prepared by twin-screw extruder. Thermal properties were investigated by experiments and molecular dynamics simulations. Differential scanning calorimetry (DSC) and thermogravimetric analysis (TGA) were used and 1.34 °C increase of the glass transition temperature (T_g) and 12 °C improvement of thermal stability were observed for PLA–silica nanocomposites as compared to neat PLA. Molecular dynamics simulations (NPT ensemble) were carried out using modified OPLS-AA force field, and T_g and root-mean-square radii of gyration (R_g) were calculated. A good agreement between the simulation results and experiments was obtained.

1. Introduction

The problems associated with the disposal of petroleum-derived plastics have raised the demand for biodegradable polymers [1]. Poly(lactic acid) (PLA) is a biodegradable aliphatic polyester derived from 100% renewable resources, such as corn and sugar beets. Moreover, it has unique physical properties that make it useful in diverse applications including paper coating, fibers, films, and packaging [2]. Currently, PLA is primarily used for medical applications such as drug delivery devices, absorbable sutures, and as a material for medical implants and other related applications [3]. Phase transition behavior, morphology, miscibility and other physical properties of PLA-based nanoscale structures have been widely studied recently [4–9].

Polymer nanocomposites have received considerable attention because of the remarkable barrier, thermal, and mechanical properties that they exhibit with respect to conventional polymer composites [10]. Incorporation of nanoscale fumed silica particles into polymers was found to increase both gas permeability and organic vapor permanent gas selectivity because fumed silica nanoparticles modified chain packing of polymers [11,12]. PLA-coated mesoporous silica nanospheres were used as fluorescence probe for detection of amino-containing neurotransmitters [13]. There is a great need to understand the underlying principles of the polymer nanocomposites at the molecular level.

Molecular dynamics (MD) simulation is a tool suited for the molecular-level study of the influence of nanoparticles on the structure and dynamics of polymers, since detailed information on the properties near the surfaces of a nanoparticle is difficult to obtain experimentally [14]. The diffusion of gases through fumed silica poly(1-trimethylsilyl-1-propyne) nanocomposite membrane was studied by molecular dynamics simulation by Zhou et al. [15]. Molecular model for the montmorillonite (clay) polymer nanocomposite was developed by Boulet et al. and Gardebien et al. [16,17]. Both experimental and molecular dynamics simulation studies have been conducted to understand different aspects of structures and properties of polymer nanocomposite. At molecular level, the interactions between silica nanoparticles and polymer and the influence of silica nanoparticles on the structure, dynamics and thermal properties of polymer are still unknown. We have studied the glass transition behavior of neat PLA using MD simulation [18]. However, there is still no reported work in the literature that uses MD simulation to study the glass transition behavior of nanofiller-modulated PLA.

This paper reports our most recent effort to examine the thermal properties of PLA fumed silica nanocomposites by both experiment and simulations, in order to expand our previous study on the subject [18]. The MD studies described in this work used the Groningen Machine for Chemical Simulation (GROMACS, version 3.3) software package [19–21]. Our results showed that fumed silica nanoparticles modified the polymer chain packing which led to an increase in the glass transition temperature (T_g) and improved thermal stability. Our experimental data were used to check the computational findings. A good agreement between the simulations and the experimental measurement was achieved. This

* Corresponding author. Tel.: +1 336 334 7620; fax +1 336 334 7417.
E-mail address: lou@ncat.edu (J. Lou).

0032-3861/$ – see front matter © 2008 Elsevier Ltd. All rights reserved.
doi:10.1016/j.polymer.2008.02.048

should provide new insight into thermal properties of polymer nanocomposites.

2. Experimental and computational methods

The PLA resin in the form of pellets under the commercial name PLA 4060D was supplied by NatureWorks (Minnetonka, MN). The surface-treated fumed silica nanoparticles under the commercial name CAB-O-SIL TS-530 was supplied by Cabot Corporation (Boston, MA). The nanocomposites were prepared by mixing the PLA resin with 2% (w/w) fumed silica in a C.W. Brabender (Newark, NJ) twin-screw extruder. The L/D ratio of the counter-rotating twin screw is 20. The samples were dry-mixed at room temperature prior to feeding into the twin screw. The twin-screw melt temperature was kept at 170 °C. The rotation speed of the screws was set at 20 rpm. The resulting PLA–silica nanocomposite samples were pelletized at the end of the twin-screw extruder.

A number of procedures were used to experimentally characterize the PLA nanocomposite samples. TA Instruments (New Castle, DE) differential scanning calorimeter (DSC) Q100 was used to measure the T_g of the polymer nanocomposite samples with a heating rate of 5 °C/min. Perkin–Elmer (Waltham, MA) TGA-7 was used for the thermogravimetric analysis (TGA) of the samples at a heating rate of 5 °C/min from 50 °C to 550 °C.

The potential energy of the chosen simulation system was calculated using the GROMACS implementation of the modified OPLS-AA force field (Eq. (1)). The force field parameters for PLA were obtained from O'Brien et al. [22] and the parameters for silica were taken from Wensink et al. [23].

$$E_{\mathrm{PE}} = \sum_{\text{bonds}} k_r(r-r_0)^2 + \sum_{\text{angles}} k_\theta(\theta-\theta_0)^2 + \sum_{\text{impropers}} k_\xi(\xi-\xi_0)^2 + \sum_{n=0}^{5} C_n(\cos(\Psi))^n + \sum_i \sum_{j>i} f_{ij}\left\{\frac{q_i q_j e^2}{r_{ij}} + 4\epsilon_{ij}\left[\left(\frac{\sigma_{ij}}{r_{ij}}\right)^{12} - \left(\frac{\sigma_{ij}}{r_{ij}}\right)^{6}\right]\right\} \quad (1)$$

The nontorsional bonded interactions are modeled by the first three harmonic terms for bond stretching, angle bending, and out of plane deformations for planar groups. The force constants for intramolecular deformations (k_r,k_θ,k_ξ) define the magnitude of the energy required to move the internal coordinates (r,θ,ξ) away from their unstrained default values (r_0,θ_0,ξ_0). The proper torsions are defined in terms of the specific dihedral angle (ψ) and Ryckaert–Bellemans potential parameter C_n, where $n = 0, 1, \ldots, 5$. The non-bonded interactions are modeled by Coulombic and 6-12 Lennard–Jones terms, where r_{ij} is the distance of two sites, q is the partial atomic charge, and σ_{ij} and ϵ_{ij} are the Lennard–Jones parameters. The scaling factor f_{ij} is 1.0 for all non-bonded interactions except for the 1,4-intramolecular interactions.

The amorphous PLA box containing 32 PLA chains of 50 monomers and the PLA fumed silica box containing 32 PLA chains of 50 monomers and 1 silica nanoparticle of 132 silicon atoms were generated using the method of shrinking box. All molecules were placed in a box that had a volume of approximately eight times the experimental volume. The shrinking procedure was performed very slowly by gradually increasing the pressure. The real density was reached after a time span of 1 ns [24]. Then, the system was equilibrated at NPT conditions for 20 ns at 550 K and 1 bar to obtain a well relaxed starting structure. The resulting periodic systems are shown in Fig. 1. For the determination of T_g, a cooling process was initiated by lowering the temperature stepwise by 50 K until a temperature of 200 K was reached. At each temperature, 2 ns NPT ensemble dynamics was carried out and the final configuration of this run was used as the starting structure for dynamics at the next (50 K lower) temperature.

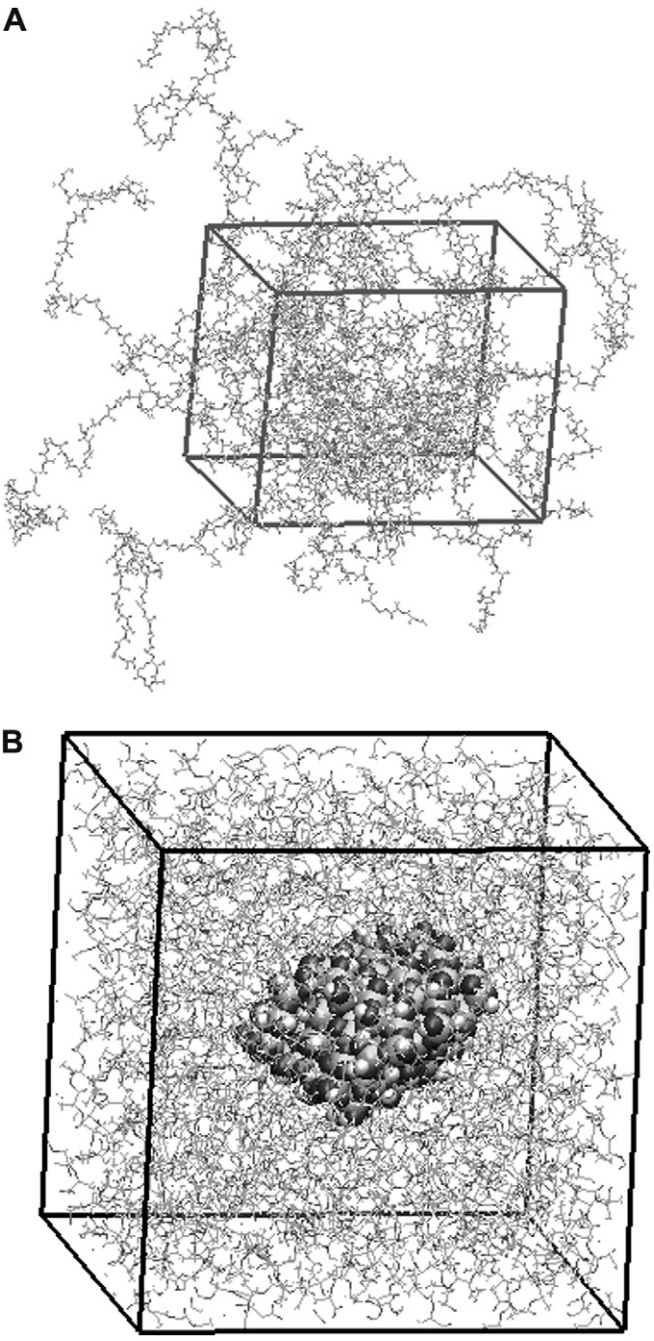

Fig. 1. Snapshots of (A) amorphous PLA box containing 32 PLA chains of 50 monomers and (B) PLA fumed silica box containing 32 PLA chains of 50 monomers and 1 silica nanoparticle of 132 silicon atoms.

All MD simulations were done using the GROMACS 3.3 simulation package on a 40-node IBM xSeries Linux Cluster. In the simulations, the leapfrog algorithm was used to integrate Newton's equations of motion with a time step of 2 fs. Periodic boundary conditions were applied. The non-bonded force calculations employed a grid system for neighbor searching. In this system, only the atoms in the neighboring grid cells were considered when building a new neighbor list. A twin-range cutoff was used for both Lennard–Jones and Coulombic calculations. A cutoff radius of 1.0 nm was used to distinguish between the short-range and the long-range forces. In the simulation, the temperature was controlled by employing a Nose–Hoover extended ensemble and the pressure was controlled by employing a Parrinello–Rahman ensemble. Initial velocities were randomly assigned from a Maxwell distribution at the

selected simulation temperature. The LINCS algorithm was used to constrain all bonds [18].

3. Results and discussion

DSC analysis was used to investigate the glass transition and crystallization/melting phenomena of neat PLA and PLA fumed silica nanocomposites prepared by the twin-screw extruder. The T_g, melting temperature (T_m) and melting enthalpy (ΔH) are summarized in Table 1. T_g is related to the chain mobility of the amorphous domains in a polymer sample. The melting temperature is related to the crystalline domains of a polymer sample. The size of the melting peak in DSC thermograms is proportional to the degree of crystallinity of a polymer sample. It can be seen from Fig. 2(A) that there was a 9 °C increase in the T_g for the PLA nanocomposites as compared to the neat PLA.

Thermal degradation can be monitored by TGA and the result is shown in Fig. 2(B) for neat PLA and PLA–silica nanocomposites.

Table 1
DSC characterization results

Sample	T_g, °C	T_m, °C	ΔH, J/g
Neat PLA	50.89	163.76	0.51
PLA with 2% fume silica	52.23	–	–

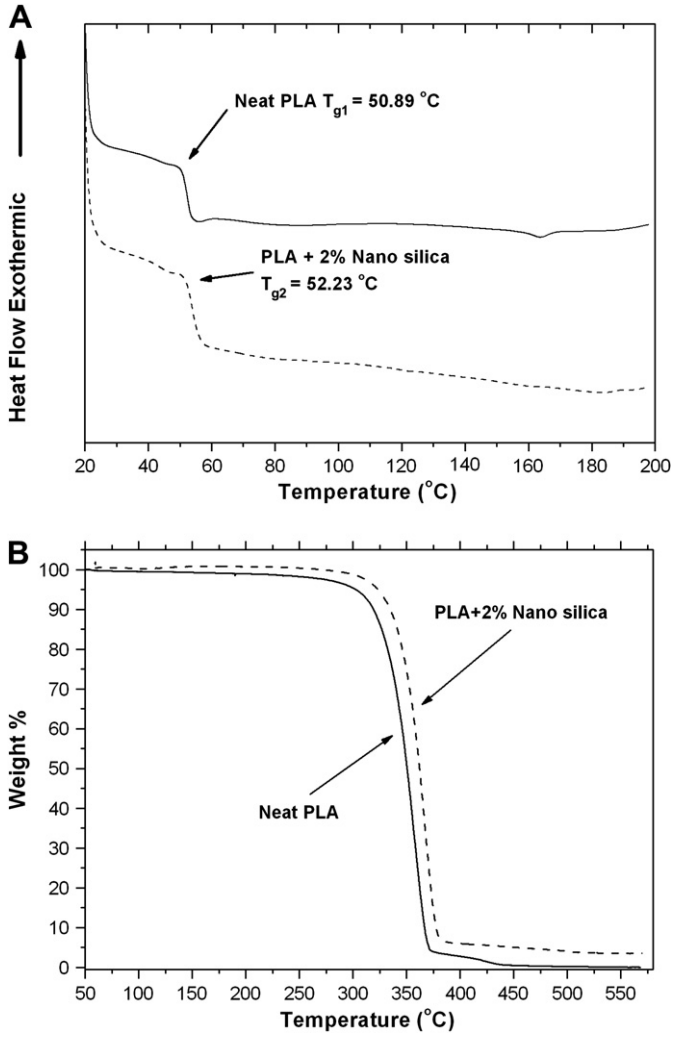

Fig. 2. (A) DSC heating thermograms recorded at 5 °C/min for neat PLA and PLA with 2% silica nanocomposite. (B) TGA traces recorded at 5 °C/min for neat PLA and PLA with 2% silica nanocomposite.

Two main reaction stages took place during the degradation of PLA. The first stage represents the decomposition of PLA chain-ends before 300 °C. The second stage, between 300 °C and 400 °C, represents the random scission of the polymer chains. In Fig. 2(B), neat PLA displayed these two reaction stages, while the nanocomposite displayed only the second stage and a 12 °C shift towards higher temperature, indicating improved thermal stability for the PLA fumed silica nanocomposites over the neat polymer. This is a common behavior observed for nanocomposites and is partly responsible for their usually improved flame-retardant properties [10].

In Fig. 3(A), the computed specific volume v is plotted as a function of temperature T. In Fig. 3(B), the computed non-bonded potential energy is plotted as a function of temperature T. The specific volume, v, is the reciprocal of the density of the box. The v values and energy values were well equilibrated for each temperature within the chosen simulation period (2 ns). Each plotted value was the average value of 200 data points sampled at each temperature for the duration of the last 1 ns (i.e., taking one data point for each 5 ps and average over 1 ns). The specific volume, v, is a function of the temperature, T. The T_g is derived as the temperature at which the slope in the v vs. T curve (i.e., dv/dT) changes [25].

It can be seen from Fig. 3(A) and (B) that the simulation predicted an increase in T_g for PLA–silica nanocomposites as compared to neat PLA. Specifically, the change in T_g was 13 °C from specific volume calculation and 15 °C from non-bonded potential energy calculation. This increase in T_g was qualitatively consistent with the experimental result of 1.34 °C (Fig. 2(A)). The two energy components were plotted as functions of temperature in Fig. 2(B) and (C). These two components played different roles in the glass transition process. We noticed that the bonded potential energy decreased linearly with decreasing temperature, which suggested that the degree of freedom for bonded interaction component was in equilibrium in both rubbery and glassy states. We also found that there was a small break at T_g in the plot of non-bonded potential energy. It appears that the non-bonded interaction component played an important role in the glass transition process.

The radius of gyration is a parameter commonly used to describe the size of a polymer chain.

$$R_g = \sqrt{\frac{\sum_i \|r_i\|^2 m_i}{\sum_i m_i}} \tag{2}$$

where m_i is the mass of atom i, and r_i the position of atom i with respect to the center of mass of the molecule. Fig. 4 shows a plot of calculated root-mean-square radii of gyration, $\langle R_g^2 \rangle^{1/2}$, as a function of temperature T for PLA chains in the matrix and PLA chains around silica nanoparticle. The average $\langle R_g^2 \rangle^{1/2}$ of PLA chains in the matrix is 1.94 nm, whereas the average $\langle R_g^2 \rangle^{1/2}$ of PLA chains around the silica nanoparticle is 1.35 nm. The average $\langle R_g^2 \rangle^{1/2}$ of silica nanoparticle is 0.93 nm. It is noted that the radii of gyration of PLA chains around the silica nanoparticle were much smaller than that of the neat PLA at the same temperature, which indicated that silica nanoparticles caused certain changes in the PLA chain packing at the polymer nanosilica interfaces. This morphological difference between the neat PLA and the PLA–silica nanocomposite was an important reason for the observed increase in T_g and the improvement over thermal stability for the PLA fumed silica nanocomposites.

In order to further analyze the structural effect the nanoparticle has on the PLA melt, the radii of gyration of PLA chains around the silica nanoparticle and PLA chains in the matrix at 500 K were calculated and the box chart is shown in Fig. 5. Starr et al. reported that

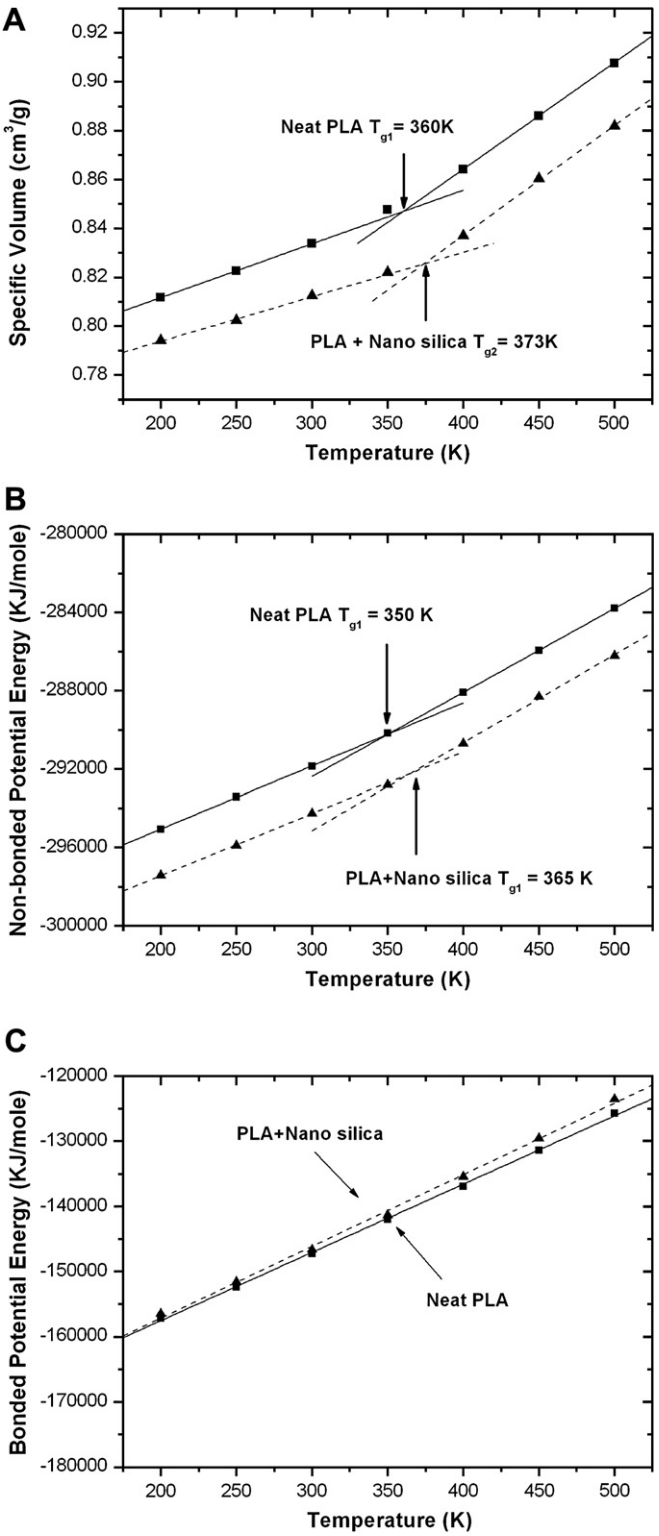

Fig. 3. (A) The plot of computed specific volume v as a function of temperature T. (B) The plot of computed non-bonded potential energy as a function of temperature. (C) The plot of computed bonded potential energy as a function of temperature.

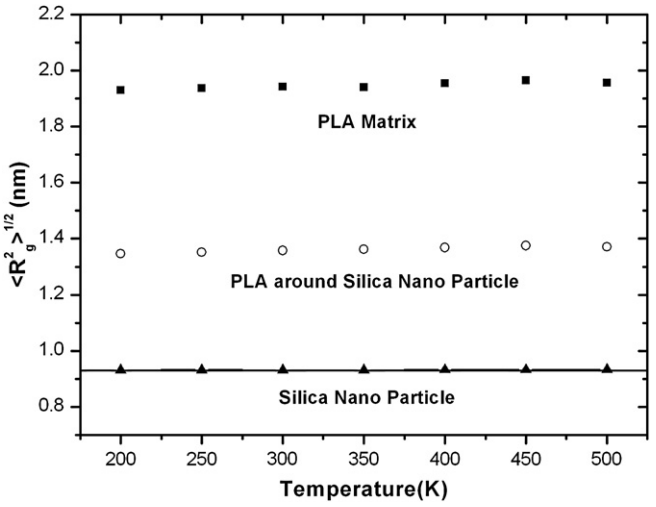

Fig. 4. The plot of the root-mean-square radii of gyration versus temperature (From top to bottom: PLA chains in the matrix, PLA around Silica Nano Particle and Silica Nano Particle).

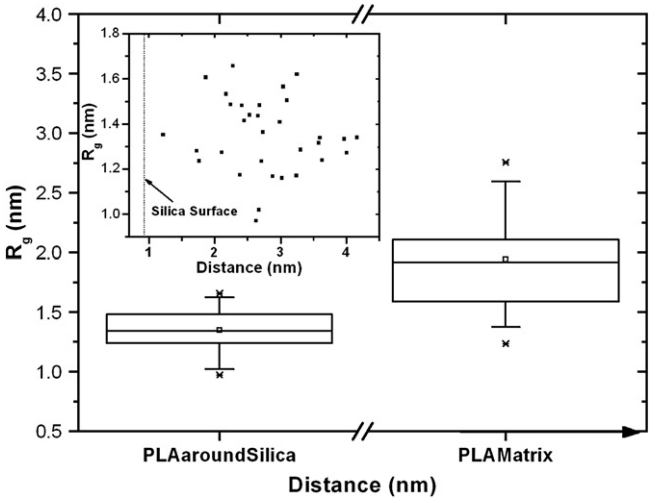

Fig. 5. Box chart of radii of gyration for PLA chains around silica nanoparticle and PLA chains in the matrix at 500 K. Inset: plot of radii of gyration as a function of distance from the silica center of mass for 32 PLA chains around silica nanoparticle surface at 500 K.

the polymer chains surrounding a nanofiller were elongated and flattened and had larger $\langle R_g \rangle$ in their simulation system, which included small polymers of $\langle R_g \rangle = 4.72$ nm and large nanofiller of $\langle R_g \rangle = 10$ nm [26]. However, for our system, the radii of gyration of PLA chains around the nanoparticle decreased because the $\langle R_g \rangle$ of nanofiller (0.93 nm) is much smaller than $\langle R_g \rangle$ of polymer chains in the matrix (1.94 nm) and the polymer was bended and compressed when they attach to the nanoparticle. The inset in Fig. 5 is the plot of radii of gyration as a function of distance from the center of mass of the silica nanoparticle for 32 PLA chains around the silica nanoparticle at 500 K. Although the radii of gyration of the PLA chains in the matrix, which are far away from the surface of the silica nanoparticle, tended to be larger than the PLA chains around the silica nanoparticle, the radii of gyration of 32 PLA chains within 4 nm distance from the center of mass of the silica nanoparticle still showed a random distribution. We also calculated the number of monomer units which were directly attached on the nanoparticle surface for each PLA chain. The plot of distance from the center of mass of the silica nanoparticle as a function of number of monomer units is shown in Fig. 6. Linear relationship was found and no attached monomers were expected if the distance from the center of mass of the nanoparticle is beyond 3 nm.

To determine the self-diffusion coefficient D_N, one can use the Einstein relation (Eq. (3)) [27].

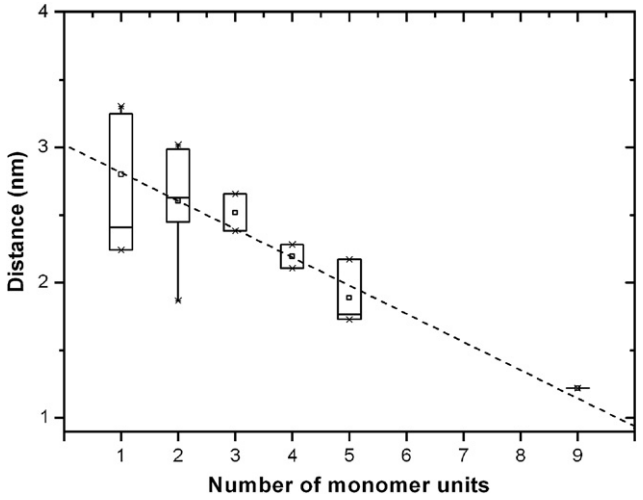

Fig. 6. Plot of distance from the silica center of mass as a function of number of monomer units which were attached on the silica nanoparticle surface for each PLA chain at 500 K.

$$\lim_{t\to\infty}\left\langle \|r_i(t)-r_i(0)\|^2 \right\rangle_{t\in N} = 6D_N t \tag{3}$$

The terms in the angular brackets represent the time averaged mean-square displacement (MSD). After approximately 100 ps, the molecules will be moving in a totally random fashion (Brownian motion), and the mean-square deviation of the system will increase linearly as the atoms drift away from each other. The MSD from 200 ps to 800 ps was fit to a linear curve and the slope is directly related to the self-diffusion coefficient. The plot of self-diffusion constant D_N as a function of temperature for PLA chains in the matrix and PLA chains around the nanoparticle is shown in Fig. 7. The self-diffusion constant D_N increased dramatically when the temperature is across T_g and the D_N decreased as PLA chains approached the surface of the nanoparticle.

The viscosity can be calculated from an equilibrium simulation using the Einstein relation [21]:

$$\eta = \frac{1}{2}\frac{V}{k_B T}\lim_{t\to\infty}\frac{\mathrm{d}}{\mathrm{d}t}\left\langle \left(\int_{t_0}^{t_0+t} P_{xz}(t')\mathrm{d}t' \right) \right\rangle_{t_0} \tag{4}$$

The shear viscosity converged when the temperature is above 500 K. And the plot of shear viscosity for PLA chains in the matrix and PLA chains around the nanoparticle is shown in Fig. 8. The shear viscosity increased when PLA chains approached the nanoparticle surface.

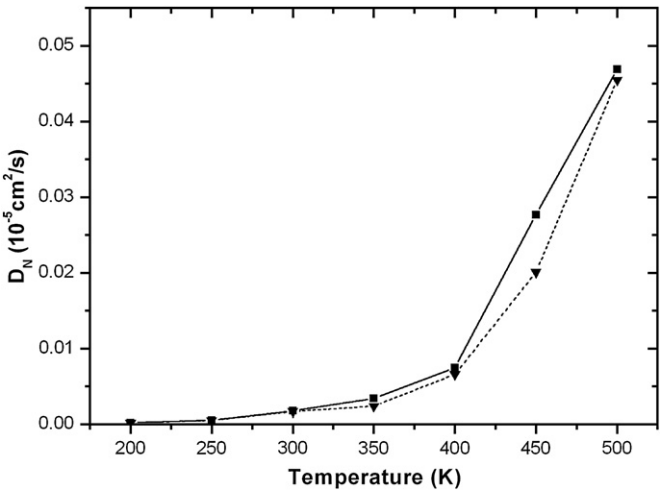

Fig. 7. Plot of self-diffusion constant D_N as a function of temperature for PLA chains in the matrix (top) and PLA chains around silica nanoparticle (bottom).

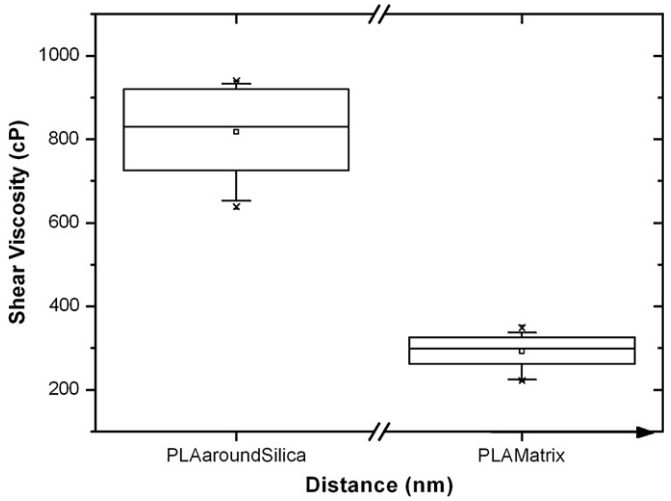

Fig. 8. Box plot of shear viscosity for PLA chains around silica nanoparticle and PLA chains in the matrix.

4. Conclusion

Poly(lactic acid) fumed silica nanocomposites were prepared by twin-screw extruder. An increase of 1.34 °C in the T_g and 12 °C improvement of thermal stability were observed for PLA–silica nanocomposites as compared to the neat PLA. The increase in T_g for PLA–silica nanocomposite was qualitatively consistent between the experimental result and the MD simulation. While the bonded interaction components appeared to have little influence, the non-bonded interaction components played an important role in the glass transition process. The radii of gyration of PLA chains around the nanoparticle decreased because the polymers were bended and compressed when they attach to the smaller nanoparticle. The self-diffusion coefficient decreased and the shear viscosity increased when PLA chains approached the surface of the nanoparticle.

Acknowledgements

This work was funded by USDA Award No. 2003-38820-14102 and DOE Grant DE-FG26-06NT42742 awarded to Dr. Lou.

References

[1] Richard AG, Bhanu K. Science 2002;297:803.
[2] Drumright RE, Gruber PR, Henton DE. Adv Mater 2000;12:1841.
[3] Uhrich KE, Cannizzaro SM, Langer RS, Shakesheff KM. Chem Rev 1999;99:3181.
[4] Sun L, Ginorio JE, Zhu L, Sics I, Rong L, Hsiao BS. Macromolecules 2006;39:8203.
[5] Lee WK, Iwata T, Gardella JAJ. Langmuir 2005;21:11180.
[6] Wang Y, Pfeffer R, Dave R, Enick R. AIChE J 2005;51:440.
[7] Rohman G, Grande D, Laupretre F, Boileau S, Guerin P. Macromolecules 2005;38:7274.
[8] Tretinnikov ON, Kato K, Iwata H. Langmuir 2004;20:6748.
[9] Rzayev J, Hillmyer MA. J Am Chem Soc 2005;127:13373.
[10] Alexandre M, Dubois P. Mater Sci Eng R 2000;28:1.
[11] Merkel TC, Freeman BD, Spontak RJ, He Z, Pinnau I, Meakin P, et al. Science 2002;296:519.
[12] Zhong J, Lin G, Wen WY, Jones AA, Kelman S, Freeman BD. Macromolecules 2005;38:3754.
[13] Radu DR, Lai CY, Wiench JW, Pruski M, Lin VSY. J Am Chem Soc 2004;126:1640.
[14] Starr FW, Schroder TB, Glotzer SC. Macromolecules 2002;35:4481.
[15] Zhou JH, Zhu RX, Zhou JM, Chen MB. Polymer 2006;47:5206.
[16] Boulet P, Coveney PV, Stackhouse S. Chem Phys Lett 2004;389:261.
[17] Gardebien F, Bredas JL, Lazzaroni R. J Phys Chem B 2005;109:12287.
[18] Zhang J, Yu L, Yan J, Lou J. Polymer 2007;48:4900.
[19] Berendsen HJC, van der Spoel D, van Drunen R. Comput Phys Commun 1995;91:43.
[20] Lindahl E, Hess B, van der Spoel D. J Mol Model 2001;7:306.

[21] van der Spoel D, Lindahl E, Hess B, van Buuren AR, Apol E, Meulenhoff PJ, et al. Gromacs user manual version 3.3, www.gromacs.org; 2005.
[22] O'Brien CP. Quantum and molecular modeling of polylactide. Ph.D. dissertation. Clemson University; 2005.
[23] Wensink EJW, Hoffmann AC, Apol MEF, Berendsen HJC. Langmuir 2000;16:7392.
[24] van der Vegt NFA, Briels WJ, Wessling M, Strathmann H. J Chem Phys 1996;105:8849.
[25] Wagner KG, Maus M, Kornherr A, Zifferer G. Chem Phys Lett 2005;406:90.
[26] Starr FW, Schroder TB, Glotzer SC. Phys Rev E 2001;64:021802.
[27] Allen MP, Tildesley DJ. Computer simulations of liquids. Oxford: Oxford Science Publications; 1987.